

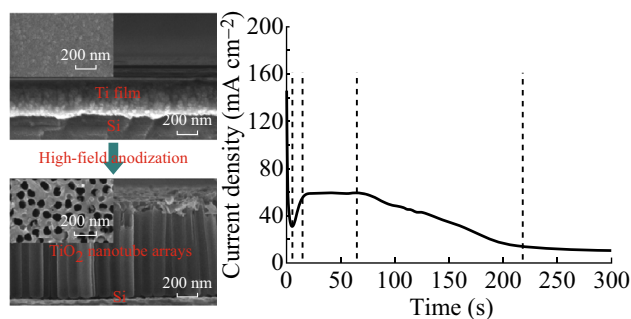
Fast Growth of Highly Ordered TiO₂ Nanotube Arrays on Si Substrate under High-Field Anodization

Jingnan Song¹ · Maojun Zheng^{1,2} · Bin Zhang¹ · Qiang Li¹ · Faze Wang¹ · Liguo Ma¹ · Yanbo Li³ · Changqing Zhu¹ · Li Ma⁴ · Wenzhong Shen¹

Received: 23 July 2016 / Accepted: 17 September 2016 / Published online: 9 November 2016
© The Author(s) 2016. This article is published with open access at Springerlink.com

Abstract Highly ordered TiO₂ nanotube arrays (NTAs) on Si substrate possess broad applications due to its high surface-to-volume ratio and novel functionalities, however, there are still some challenges on facile synthesis. Here, we report a simple and cost-effective high-field (90–180 V) anodization method to grow highly ordered TiO₂ NTAs on Si substrate, and investigate the effect of anodization time, voltage, and fluoride content on the formation of TiO₂ NTAs. The current density–time curves, recorded during anodization processes, can be used to determine the optimum anodization time. It is found that the growth rate of TiO₂ NTAs is improved significantly under high field, which is nearly 8 times faster than that under low fields (40–60 V). The length and growth rate of the nanotubes are further increased with the increase of fluoride content in the electrolyte.

Graphical Abstract Highly ordered TiO₂ nanotube arrays (NTAs) on Si substrate have been fabricated by high-field anodization method. A high voltage (90–180 V) leads to a high growth rate of TiO₂ NTAs (35–47 nm s⁻¹), which is nearly 8 times faster than the growth rate under low fields (40–60 V). Furthermore, the current density–time curves recorded during the anodization provide a facial method to determine the optimal anodization parameters, leading to an easy obtaining of the desired nanotubes.



✉ Maojun Zheng
mjzheng@sjtu.edu.cn

¹ Key Laboratory of Artificial Structure and Quantum Control, Ministry of Education, Department of Physics and Astronomy, Shanghai Jiao Tong University, Shanghai 200240, People's Republic of China

² Collaborative Innovation Center of Advanced Microstructures, Nanjing 210093, People's Republic of China

³ Institute of Fundamental and Frontier Sciences, University of Electronic Science and Technology of China, Chengdu 610054, People's Republic of China

⁴ School of Chemistry and Chemical Technology, Shanghai Jiao Tong University, Shanghai 200240, People's Republic of China

Keywords TiO₂ nanotube arrays · Si substrate · Anodization · High field · Controllable preparation

1 Introduction

Since the first report on the growth of highly ordered TiO₂ nanotube arrays (NTAs) by a simple electrochemical anodization method in 1999 [1], TiO₂ NTAs prepared by electrochemical anodization of titanium foil and alloys have attracted much attention in various applications, such as corrosion protection [2, 3], sensors [4–6], dye-sensitized solar cells [7], photocatalysis [8–11], biomedical [12, 13], and Li-ion batteries [14]. The morphology and growth rate of NTAs can be easily controlled through optimization of anodization parameters, such as anodization voltage, time, and electrolyte composition [15–17]. The formation of TiO₂ NTAs is a competition consequence between oxidation of titanium and electric-field-induced etching of TiO₂ as well as chemical etching of TiO₂ by fluoride ion [16, 18]. In the electrolytes, fluoride ions are believed to play an important role in the formation of nanotubular array, and three different fluoride-containing electrolytes have been developed. Dilute hydrofluoric acid (HF) aqueous solution is the first one used in anodization of titanium. However, the maximum thickness of TiO₂ NTAs was limited to only several hundred nanometers due to the fast chemical dissolution of TiO₂ NTAs by fluoride ions in aqueous solution [19]. Later, TiO₂ NTAs with a thickness of a few micrometers were obtained in fluoride-containing buffer solution, in which the dissolution rate of formed TiO₂ NTAs was reduced [20, 21]. Recently, a nonaqueous electrolyte composed of ammonium fluoride (NH₄F) and a viscous organic electrolyte, such as ethylene glycol (EG) or glycerol was used, and the length of TiO₂ NTAs was increased to several hundred microns [22–24].

To our knowledge, most of the previous works are focused on the fabrication of TiO₂ NTAs on titanium foils. TiO₂ NTAs on titanium foils have poor mechanical properties, that is, they are easily cracked and detached when subjected to stress on titanium foils [25]. In addition, when TiO₂ NTAs on titanium foils are assembled into functional devices, the metal electrodes deposited on the oxide layer may diffuse into the titanium foil at elevated temperatures, which may cause an electrical short circuit. Most importantly, titanium foil underneath the oxide layer has thickness of 0.1–1 mm, making it incompatible for use in micro-electronic device [26, 27]. Thus, it is of great significance to form TiO₂ NTAs directly on functional substrates [28]. So far, there are many reports about fabrication of TiO₂ NTAs films on both conductive (ITO glass and Si) [29–31] and nonconductive (SiO₂ and glass) substrates [27, 32–34].

These nanotubular structures were fabricated by anodizing titanium film under low fields (10–60 V). For example, Samira et al. [34] have fabricated ordered TiO₂ NTAs on Si substrate under low field (40 V), where a long anodization time was required. Nevertheless, it is still a challenge to obtain high-quality TiO₂ NTAs efficiently on Si substrate under high fields. Kim et al. [27] prepared highly ordered TiO₂ NTAs by anodization of as-prepared titanium films which were deposited on patterned Si substrate. They also investigated the influence of the quality of titanium film and high anodization voltages (up to 200 V) on the morphology of TiO₂ NTAs. However, the pre-patterning technique is limited because of its expense and the need for external treatments to achieve highly ordered TiO₂ NTAs films. According to Ono et al. [35], the condition of high current density, i.e., a high electric field, is the key factor that determines the self-ordering of the pore arrangement.

Here, based on a high-field anodization technique we previously developed [36, 37], a 938-nm-thick TiO₂ NTAs with high quality was achieved via anodizing titanium film on Si substrate at 120 V for 20 s, which is a significant improvement in growth rate. The effect of anodization time, applied voltage, and NH₄F contents on the morphology and growth rate of TiO₂ NTAs were systematically investigated. The current density measured over the entire anodization time was recorded, which can provide a way to understand the whole anodization process and estimate the termination time of anodization of titanium film. Finally, the effect of annealing temperatures on crystalline structure was examined.

2 Experimental Details

2.1 Ti Thin-Film Deposition on Si Substrate

The n-type Si (100) wafers were degreased by successively sonicating in acetone and ethanol for 10 min to remove contaminants followed by rinsing in deionized (DI) water, and then dried in nitrogen. Titanium film with a thickness of 360–530 nm was deposited on Si substrate by direct current (DC) magnetron sputtering in which titanium target with 99.999 % purity was used. The sputter chamber was pumped down to 4.0×10^{-4} Pa. Argon gas was purged into the chamber and maintained at 0.52 Pa during the deposition process. The Si substrate was kept at room temperature. The titanium film was deposited at 150 W for 10 min.

2.2 Synthesis of TiO₂ NTAs on Si Substrate

TiO₂ NTAs were synthesized via an electrochemical anodization process, where a two-electrode configuration with graphite plate was used as cathode and titanium film as anode. The electrolyte was stirred at 800 rpm for heat dissipation during the reaction. A uniform local voltage was produced by a regulated DC power supply (Agilent Technologies N5752A). For the first set of experiment, the anodization time was varied from 2 to 120 s, whereas the anodization voltage was kept at 90 V and an organic electrolyte was kept invariant containing 0.3 wt% NH₄F, 96 vol% EG, and 4 vol% DI water. For the second set of experiment, the anodization voltage was varied from 40 to 180 V, whereas the anodization time was fixed at 20 s and the electrolyte was kept the same. The above experiments were all performed at two temperatures of 20 and 0 °C. For the third set of experiment, NH₄F content of the electrolyte was varied from 0.2 to 0.4 wt%, and the anodization was performed at 120 V for 15 s. The as-grown TiO₂ NTAs on Si substrate were annealed at different temperatures (350, 550, and 750 °C). The details of the anodization parameters for three different sets of TiO₂ NTAs are summarized in Table 1.

2.3 Characterization

The morphologies of TiO₂ NTAs were examined using field-emission scanning electron microscope (SEM, Zeiss Ultra Plus FESEM), equipped with an energy dispersive X-ray (EDX) analyzer. EDX measurements were conducted at 10 keV to analyze the elemental composition of TiO₂ NTAs on Si substrate. The crystallinity of TiO₂ NTAs was investigated by X-ray diffraction analysis (XRD, D8 Discover with GADDS, Bruker Advanced X-ray Solutions, Inc.). Raman spectra were measured using the 514 nm of an Ar⁺ laser as the exciting light source (Jovin Yvon Labram 800002).

3 Results and Discussion

3.1 Formation of TiO₂ NTAs on Si Substrate

Figure 1 shows the top and side view of the titanium film. It can be seen from Fig. 1a that the top of the film is

covered with good packing of particles, producing a dense and smooth film. A side view with high density is shown in Fig. 1b. Figure 2 displays the morphologies and corresponding EDX analysis of the as-anodized TiO₂ NTAs fabricated at 150 V for 20 s. As shown in Fig. 2a, the surface is covered by pronounced grains, and the non-tubular layers above the tubes can be observed from the cross-sectional image (Fig. 2b). In order to remove the grains on the surface, the prepared samples were immersed into a 0.05 wt% HF aqueous solution for 25 min, and the images of the immersed sample are presented in Fig. 2c, d. It can be seen, the grains disappear after the immersion process, whereas the tubular structure appears. The TiO₂ NTAs have an average diameter of ~80 nm and a nanotube length of ~750 nm. When the immersion time was increased to 40 min, TiO₂ NTAs peeled off from Si substrate completely, and only TiO₂ NTAs remained (see Fig. 2e). This may be due to the chemical dissolution of the fluoride-rich TiO₂ layer between the TiO₂ NTAs and substrate when exposed to HF aqueous solution for a long time [38–40]. Therefore, all subsequent samples were immersed in a 0.05 wt% HF aqueous solution for 25 min to keep good adhesion of TiO₂ NTAs on the substrate, even annealing at high temperature.

EDX measurements were conducted to analyze the elemental composition of TiO₂ NTAs on Si substrate. Figure 2f shows the EDX spectra of the sample depicted in Fig. 2c, where some characteristic peaks of Ti, O, and Si appear. Figure 2g shows the EDX spectra of the sample displayed in Fig. 2e. Only Ti and Si peaks were observed, demonstrating that TiO₂ NTAs were removed from the substrate completely after immersion for 40 min.

3.2 Effect of Anodization Time on the Morphology of TiO₂ NTAs

In order to better understand the anodization process, the current density–time (*I*–*t*) curve was recorded during anodization at 90 V (see Fig. 3). There are five stages in the anodization process. Firstly, the titanium film is oxidized under high field and a compact TiO₂ barrier layer is formed (Fig. 4a). The high current density decays initially with increasing oxide thickness. Secondly, nanopores are formed as shown in Fig. 4b. These primary pores appear at

Table 1 Details of anodization parameters for three different sets of TiO₂ NTAs

	Set (1) variation of anodization time	Set (2) variation of applied voltage	Set (3) variation of NH ₄ F contents
Anodization time (s)	2–120	20	15
Applied voltage (V)	120	40–180	120
The contents of NH ₄ F (wt%)	0.3	0.3	0.2–0.4

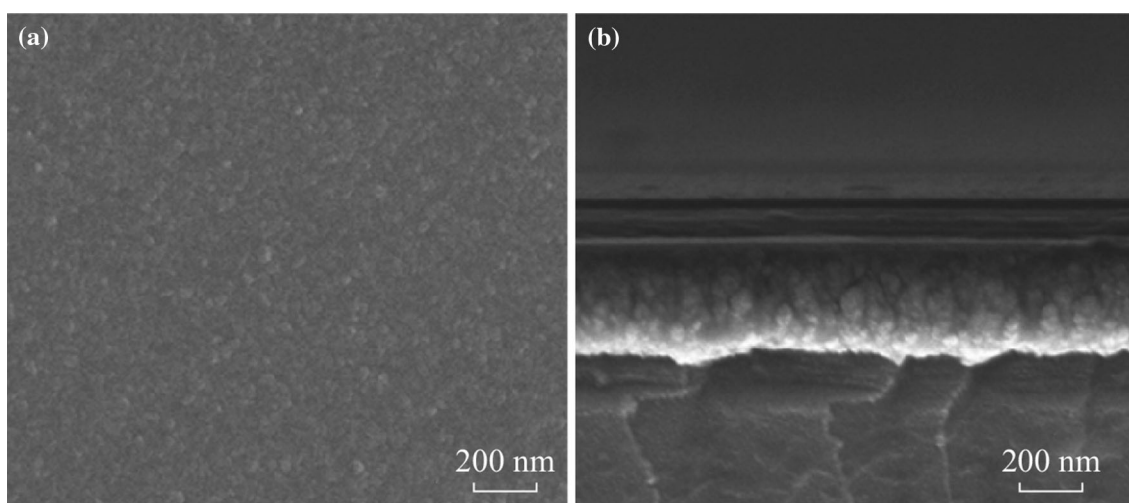


Fig. 1 SEM images of *top* view (a) and cross section (b) of Ti film deposited by the direct current magnetron sputtering

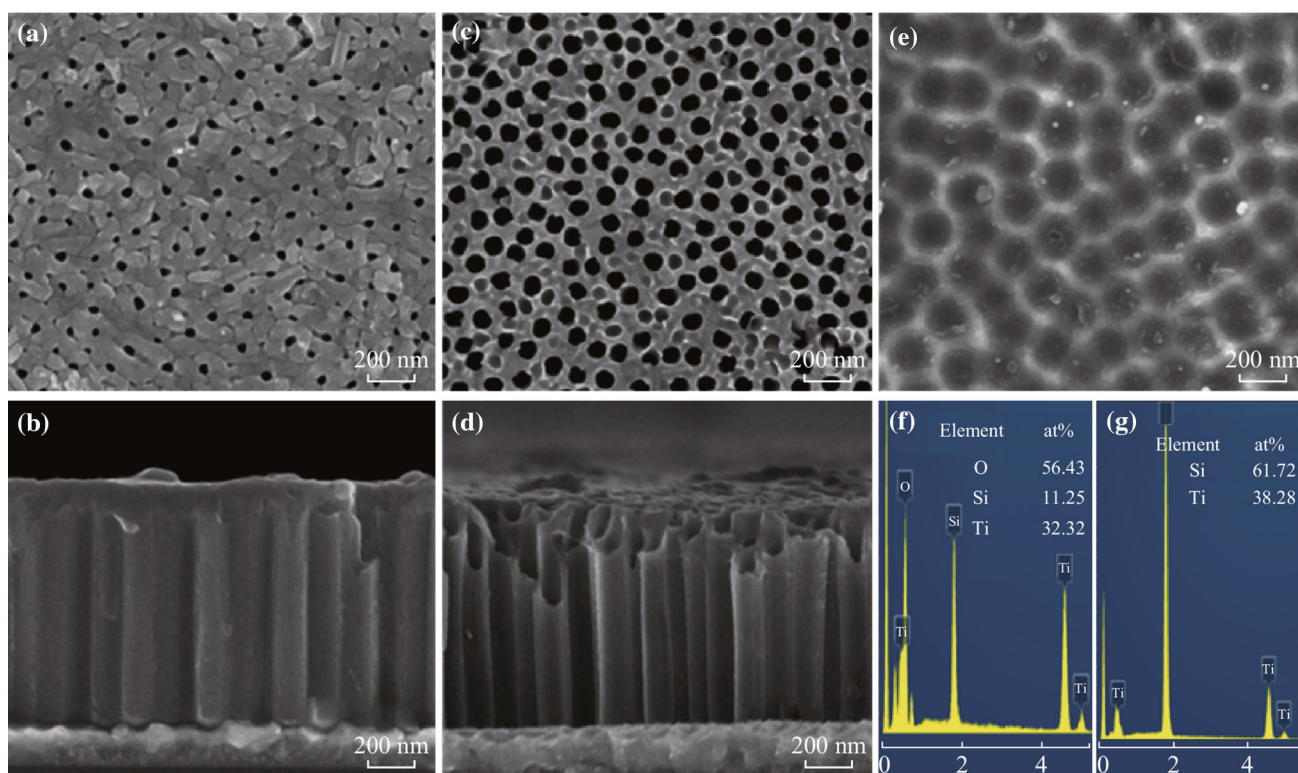


Fig. 2 The *top* (a) and *side* view (b) of TiO₂ NTAs on Si substrate formed at 150 V for 20 s. The *top* (c) and *side* view (d) of the sample immersed in a 0.05 wt% HF aqueous solution for 25 min. e The *top* view of the sample immersed in a 0.05 wt% HF aqueous solution for 40 min. f, g The EDX spectra of the sample shown in Fig. 2c, e, respectively

the titanium grain boundaries due to the dissolution of the oxide layer, which causes a localized decrease in the oxide thickness and an increase in the current density. The third stage is a steady state established a few seconds later. This is due to the dynamic equilibrium between the titanium oxidation and electric-field-induced etching of TiO₂ as well as chemical etching of TiO₂ by fluoride ion. In this stage, the tubes grow longer with increasing time (Fig. 4c–f),

whereas the thickness of the barrier layer is unchanged. As the anodization proceeds, the titanium film below the oxide layer is progressively consumed. Beyond a certain stage, the titanium film becomes discontinuous, creating highly resistant electric current pathways. Hence, the current density exhibits a decreasing trend in the fourth stage. Due to the vanishing of the titanium film, the corrosion of Si substrate and dissolution of TiO₂ become dominant. The

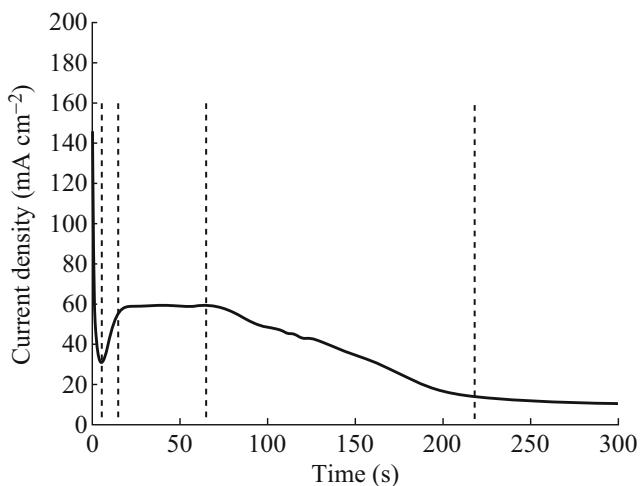


Fig. 3 The I - t curve during the anodic growth of TiO_2 NTAs at 90 V

dissolution rate of TiO_2 is faster than the oxidation rate of Ti, resulting in the decrease of TiO_2 NTAs thickness (Fig. 4g, h). In the last stage, the current density reaches a steady state again. During this stage, there was no titanium film left for oxidation, and the current is attributed to the corrosion of silicon. Therefore, close monitoring of the current response during anodization can provide a simple method to determine the optimum anodization time.

Figure 5 illustrates how the length of TiO_2 NTAs changes with the anodization time. The detailed SEM micrographs of TiO_2 NTAs obtained at different anodization times are given in Fig. 4. After anodization for 2 s, no nanotubes are observed (Fig. 4a). After 10 s, the thickness of anodic film is about 370 nm, but the nanotubes are not well-defined (Fig. 4c). Nanotubes are clearly visible after 20 and 40 s (Fig. 4d, e), their length being about 700 and

1070 nm, respectively. It can be observed that the nanotube length is longer than the thickness of the deposited titanium film, which could be due to the volume expansion during anodization [32, 33]. When the anodization time was extended to 60 s, the anodic nanotubes become longer. But with anodization time increasing to 90 s, the length of TiO_2 NTAs decreases to 930 nm (Fig. 4g). For longer anodization times, there was only little titanium film left. The oxidation of Si substrate and the dissolution of TiO_2 NTAs become dominant, causing the decrease of TiO_2 NTAs thickness. Despite the corrosion of Si, the mechanical adhesion of TiO_2 NTAs was not affected. Even after sonicating for 10 min, the TiO_2 NTAs exhibit good adhesion to the Si substrate (result not shown here).

3.3 Effect of Applied Voltage on the Morphology of TiO_2 NTAs

Figure 6 shows the SEM images of TiO_2 NTAs formed at high voltages (90–180 V), demonstrating the change in the average diameter and growth rate of nanotubes. As shown in top views (Fig. 6a, c, e, g), the pore diameter of TiO_2 NTAs under different voltages ranges from 70 to 100 nm. TiO_2 NTAs formed at 120 V have a larger pore diameter of ~ 100 nm, while TiO_2 NTAs obtained at 90 V have a smaller diameter of ~ 70 nm. Figure 7 presents the side view of TiO_2 NTAs under low fields (40 and 60 V). The growth rate (R) of TiO_2 NTAs can be calculated using the formula $R = h/t$. Here, h means the thickness of the film, which can be measured from the SEM images (Fig. 6b, d, f, h, and 7), and t is the growth time. In our experiments, the growth rate of TiO_2 NTAs under high fields is varied from 35 to 47 nm s^{-1} , which is about 8 times faster than

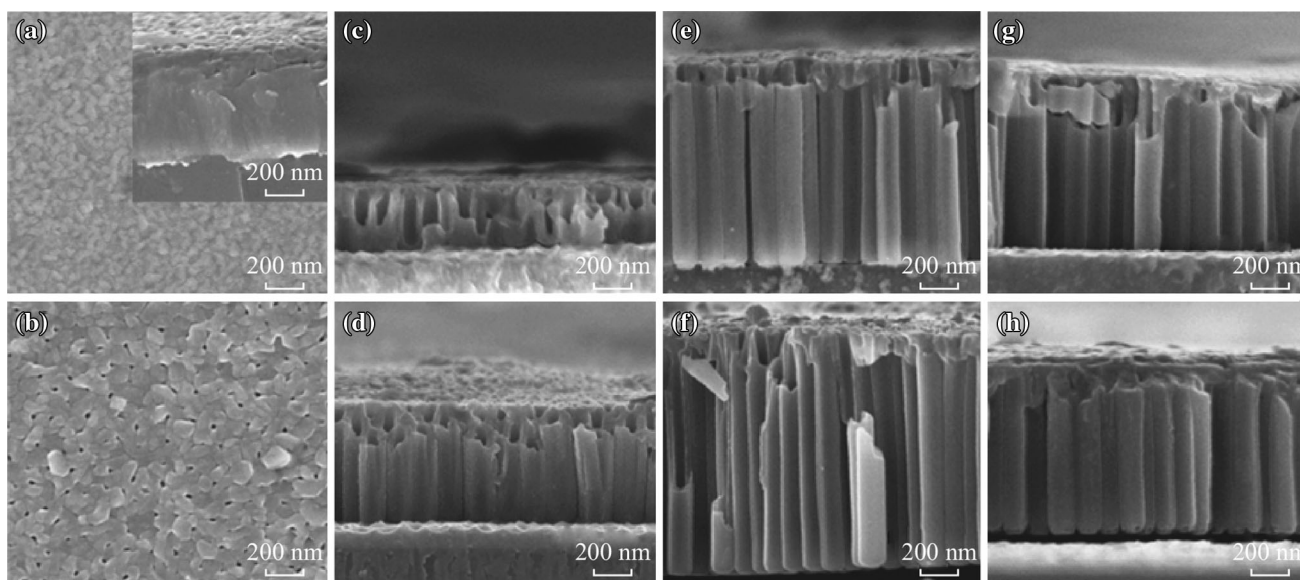


Fig. 4 SEM images of TiO_2 NTAs prepared at different anodization time **a** 2 s, **b** 7 s, **c** 10 s, **d** 20 s, **e** 40 s, **f** 60 s, **g** 90 s, and **h** 120 s

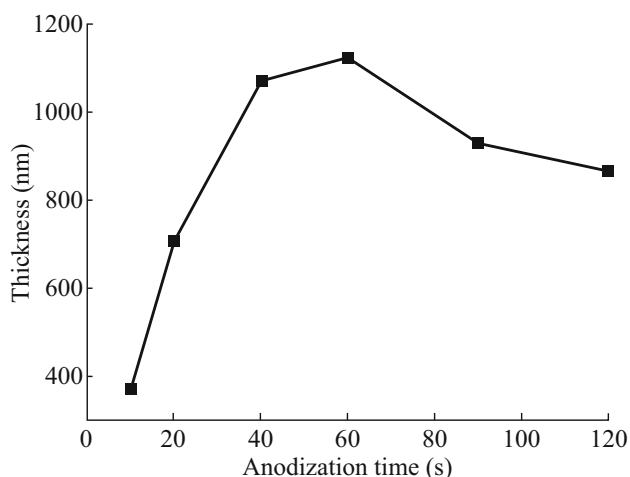


Fig. 5 Dependence of the thickness of TiO₂ NTAs formed at 90 V on the anodization time

that under low fields (40 and 60 V). And TiO₂ NTAs anodized at 120 V exhibit a maximum growth rate of $\sim 47 \text{ nm s}^{-1}$. The growth rate under different voltages is shown in Table 2.

Figure 8 shows the $I-t$ curves during the anodic fabrication of TiO₂ NTAs under different voltages (90–180 V). The inset in Fig. 8 presents the $I-t$ curves recorded under low fields (40 and 60 V). It can be found that the $I-t$ curves reveal a similar changing trend. When anodization is performed at the same electrolyte temperature (20 °C), the steady-state current density increases with increasing applied voltages (40–120 V) (see Fig. 8 and its inset) [18, 41], and a higher current density leads to a higher growth rate, which is in line with the results shown in Table 2. However, there is a deviation at higher fields (150

and 180 V), which is attributed to the lower electrolyte temperatures (0 °C). During high-field anodization, it can produce much reaction heat, which is detrimental to the quality of TiO₂ NTAs. Thus, at higher voltages (150 and 180 V), the electrolyte temperature was lowered to 0 °C. As mentioned above, TiO₂ NTAs formation is a competition between the oxidation of Ti and field-enhanced dissolution of TiO₂ as well as chemical dissolution of TiO₂ by fluoride ions. Although the oxidation of Ti and electric-field-induced etching of TiO₂ were enhanced at higher voltages, the mobility of fluoride ions in the viscous EG electrolyte was largely suppressed at lower temperatures (0 °C) [42], resulting in much lower chemical etching of TiO₂ and a thicker barrier layer at the metal/oxide interface. During the anodization, the oxidation rate decreases as the barrier layer grows [43]. Consequently, TiO₂ NTAs anodized at 150 and 180 V exhibit a lower current density than that anodized at 120 V. To check the reproducibility of the results, we have repeated the experiments conducted under different voltages (40–180 V) for three times. The average steady-state current density for each experiment has been listed in Table 3, which indicates that the result is repeatable.

3.4 Effect of Fluoride Content on the Morphology of TiO₂ NTAs

In the electrolyte, fluoride ions play an important role in the nanotubular array formation. Figure 9 shows the SEM micrographs of TiO₂ NTAs grown in electrolytes containing different fluoride contents (0.2–0.4 wt%). It can be seen that the pore diameters are varied from 85 to 95 nm,

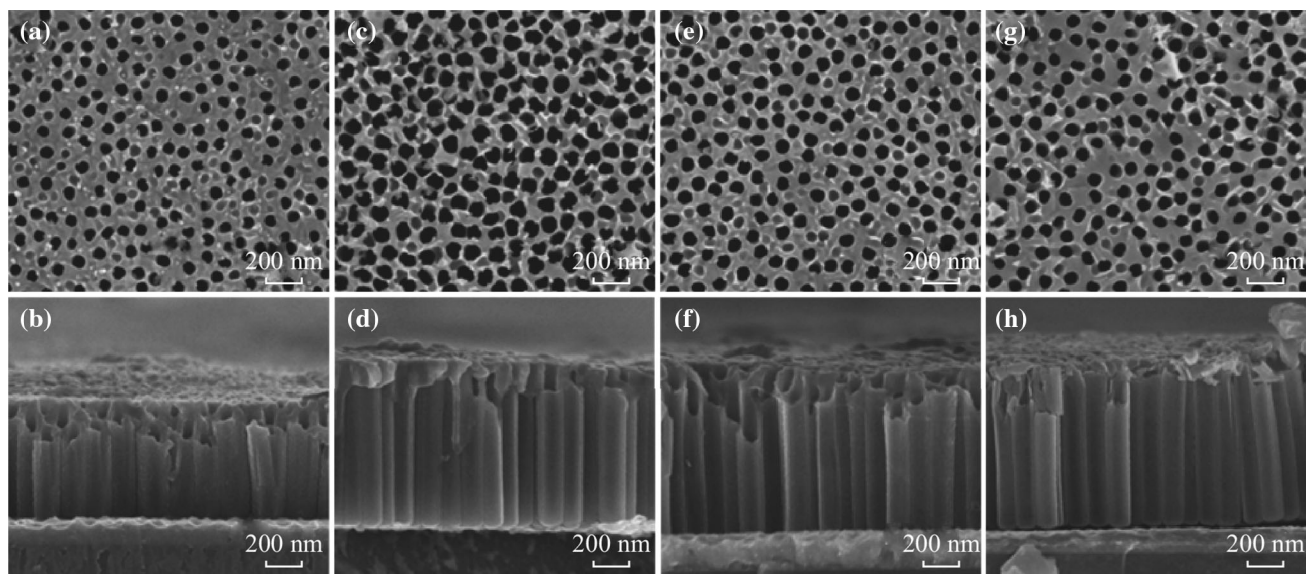


Fig. 6 The top view of TiO₂ NTAs grown at different anodization voltages for 20 s: a 90 V, c 120 V, e 150 V, and g 180 V. b, d, f, h The corresponding side view

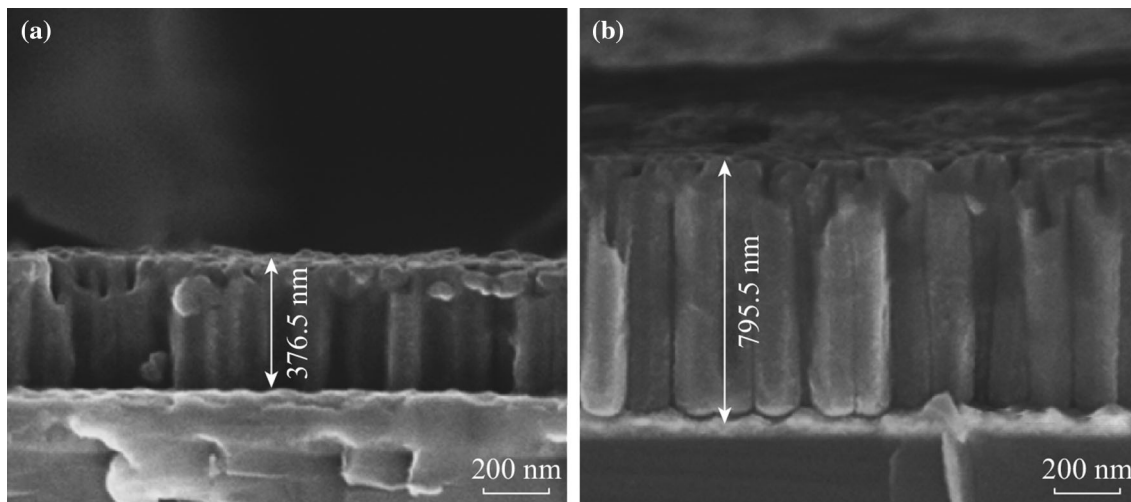


Fig. 7 SEM micrographs of TiO₂ NTAs fabricated at low fields for 150 s: **a** 40 V and **b** 60 V

Table 2 Growth rate of TiO₂ NTAs grown via anodization under different voltages

	40 V	60 V	90 V	120 V	150 V	180 V
Anodization temperature (°C)	20	20	20	20	0	0
Anodization time (s)	150	150	20	20	20	20
Growth rate of TiO ₂ NTAs (nm s ⁻¹)	3	5	35	47	37	43

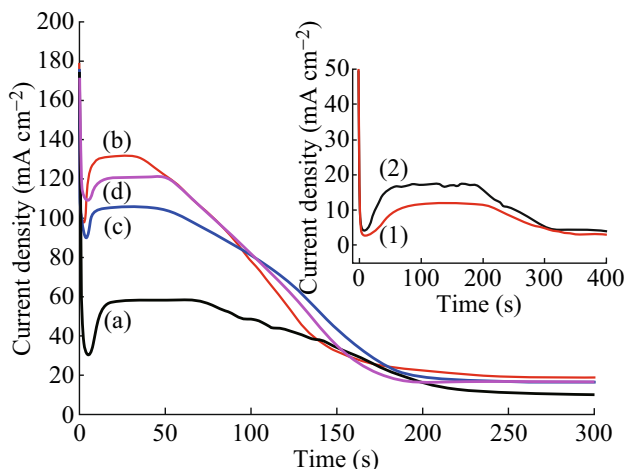


Fig. 8 The *I-t* curves during the anodic growth of TiO₂ NTAs under high voltages *a* 90 V, *b* 120 V, *c* 150 V, and *d* 180 V. The *inset* plots the *I-t* curves under low fields (1) 40 V and (2) 60 V. The experiments were carried out at two temperatures (20 °C for 40–120 V, and 0 °C for 150 and 180 V)

and no substantial change in pore diameter can be found with change in concentration (Fig. 9a, c, e). This result is in consistence with previous studies [18, 44]. Upon increasing the NH₄F content, the length of TiO₂ NTAs exhibits an increasing trend [18, 45, 46], ranging from 766 to 1285 nm (Fig. 9b, d, f).

Figure 10 presents the *I-t* curves during the anodic growth of TiO₂ NTAs in electrolytes containing

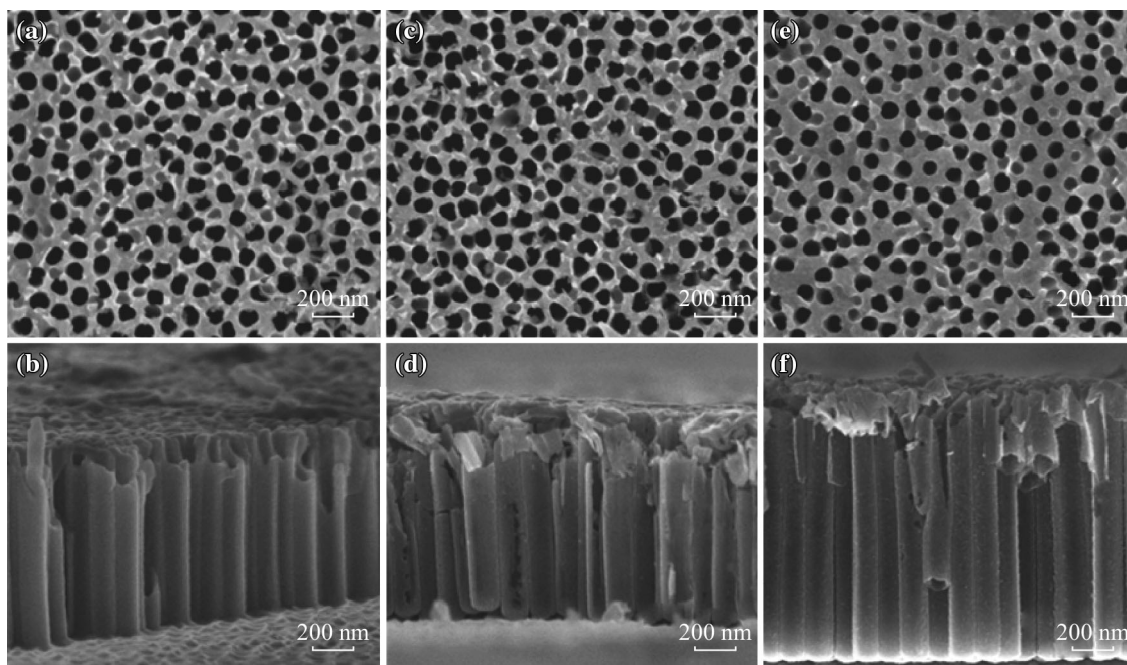
different fluoride contents. It can be observed that the increase in fluoride concentration causes an increase in the recorded current density. Pena et al. have reported that the current density is a product of three different currents associated with the ion transport through the film (Ti⁴⁺, O²⁻, and F⁻) [24]. The increase in current density with higher fluoride content may be associated with an increase of the F⁻ transport. Since the current density is generally proportional to the growth rate, the fluoride contents have a significant impact on the growth rate, and a higher fluoride concentration leads to a higher growth rate, which is consistent with the above conclusions.

3.5 Effect of Annealing Temperatures on Phase Structure

The change of crystalline structure of TiO₂ NTAs annealed at different temperatures is shown in the XRD patterns (see Fig. 11). The XRD pattern of the pre-treatment sample (Fig. 11a) reveals that the nanotubular structure mostly consists of (002) Ti, indicating that the tubes are mostly amorphous prior to annealing. After annealing at 350 °C, typical peaks of anatase phase at 2θ near 25.3°, 48°, 54°, and 55° are observed in the XRD pattern (Fig. 11b), which correspond to the planes (101), (200), (105), and (211), respectively. For thermal

Table 3 The average steady-state current density for each experiment conducted under different voltages

	Anodization temperature (°C)	Experiment times	Steady state current (mA cm ⁻²)
40 V	20	1	11.6
		2	11.9
		3	11.7
60 V	20	1	16.7
		2	16.9
		3	17.0
90 V	20	1	58.2
		2	57.9
		3	58.3
120 V	20	1	131.4
		2	130.9
		3	131.0
150 V	0	1	104.9
		2	105.3
		3	104.9
180 V	0	1	119.9
		2	120.3
		3	120.1

**Fig. 9** The *top* view of TiO₂ NTAs obtained by anodizing in electrolyte containing different NH₄F contents **a** 0.2 wt%, **c** 0.3 wt% and **e** 0.4 wt% NH₄F. **b**, **d**, **f** The corresponding *side* view

annealing at 550 °C, the intensity of anatase peaks increases. It is evident that increasing the annealing temperature leads to an increase of crystallinity. For higher temperatures (750 °C), the rutile peak (110) at around

27.4° can be observed [47, 48]. With an increase of the annealing temperature, the Ti peak intensity decreases. Annealing in air supplements the oxidation of unanodized Ti and reduces the Ti peak intensity [33].

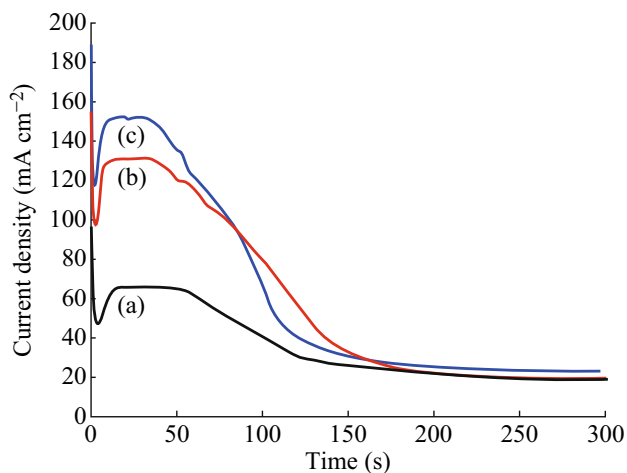


Fig. 10 The $I-t$ curves during the anodic growth of TiO_2 NTAs at 120 V in electrolytes containing different NH_4F contents **a** 0.2 wt%, **b** 0.3 wt%, and **c** 0.4 wt%

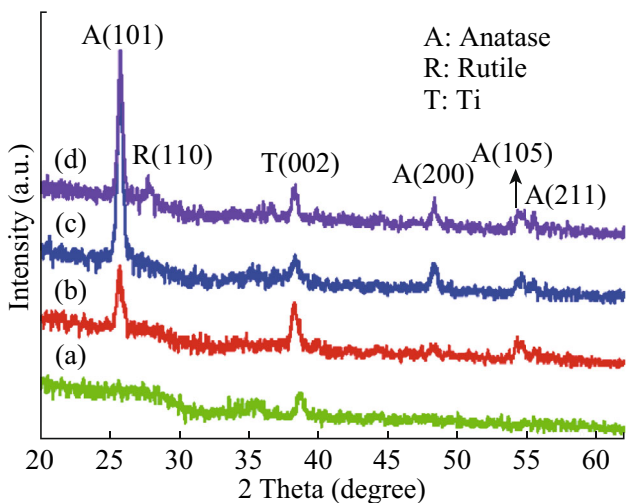


Fig. 11 XRD patterns of TiO_2 NTAs without heat treatment (**a**) or annealed at 350 °C (**b**), 550 °C (**c**), and 750 °C (**d**)

Raman spectra were employed to confirm the crystalline structure of TiO_2 NTAs. The typical Raman spectra of TiO_2 NTAs annealed at different temperatures are shown in Fig. 12. The Raman spectroscopy of unannealed samples (Fig. 12a) shows a broad spectrum, demonstrating that the unannealed sample is amorphous. When the sample was annealed at 350 °C, TiO_2 NTAs exhibit specific peaks at 143, 395, and 638 cm^{-1} , which are signatures of the anatase TiO_2 [49]. With increasing the annealing temperature from 350 to 550 °C, the anatase TiO_2 NTAs shows higher crystallinity. After annealing at 750 °C, Raman peaks observed at 443 and 608 cm^{-1} suggest that rutile is also present in the sample [50, 51]. The Si substrate signal can be identified by the

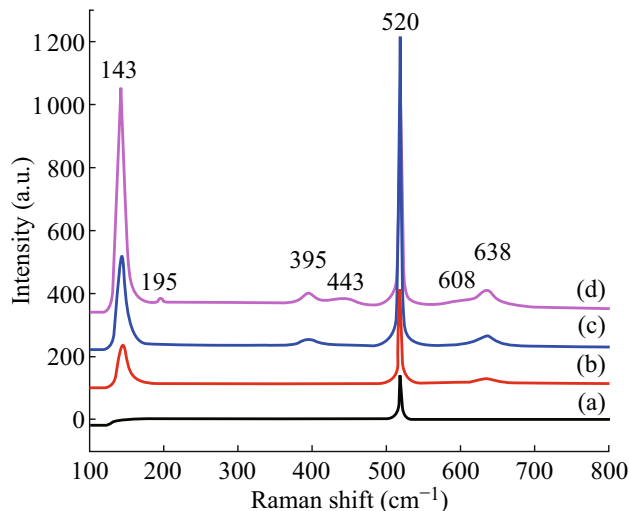


Fig. 12 Room-temperature Raman spectra of TiO_2 NTAs annealed at different temperatures **a** unannealed, **b** 350, **c** 550 °C, and **d** 750 °C

Raman peak at 520 cm^{-1} . This conclusion is in agreement with that observed from XRD patterns.

4 Conclusion

In conclusion, highly ordered TiO_2 NTAs have been obtained by high-field anodization of the Ti films deposited on Si substrate. It is found that the anodization voltage has a significant impact on the growth rate. A high voltage (90–180 V) leads to a high growth rate of TiO_2 NTAs (35–47 nm s^{-1}), which is nearly 8 times faster than the growth rate under low fields (40–60 V). When the applied voltage is 120 V, the anodization time is as short as 20 s for obtaining 938-nm-thick TiO_2 NTA with high quality, which is a significant improvement in growth rate. Additionally, the fluoride content in the electrolyte will increase the length and growth rate, but has little influence on the pore diameter. Furthermore, the $I-t$ curves measured over the entire anodization duration provide a facial method to monitor the anodization process and determine the optimum anodization time, leading to an easy obtaining of the desired nanotube arrays. Our work is anticipated to provide a way to fabricate highly ordered nanostructures on different functional substrates.

Acknowledgments This work was supported by National 863 Program 2011AA050518, the Natural Science Foundation of China (Grant Nos. 11174197, 11574203, and 61234005).

Open Access This article is distributed under the terms of the Creative Commons Attribution 4.0 International License (<http://creativecommons.org/licenses/by/4.0/>), which permits unrestricted use,

distribution, and reproduction in any medium, provided you give appropriate credit to the original author(s) and the source, provide a link to the Creative Commons license, and indicate if changes were made.

References

- V. Zwillling, E.D. Ceretti, A.B. Forveille, D. David, M.Y. Perrin, M. Aucouturier, Structure and physicochemistry of anodic oxide films on titanium and TA6 V alloy. *Surf. Interface Anal.* **27**(7), 629–637 (1999). doi:[10.1002/\(SICI\)1096-9918\(199907\)27](https://doi.org/10.1002/(SICI)1096-9918(199907)27)
- E.A. Ferreira, R.C. Rocha-Filho, S.R. Biaggio, N. Bocchi, Corrosion resistance of the Ti–50Zr at.% alloy after anodization in different acidic electrolytes. *Corros. Sci.* **52**(12), 4058–4063 (2010). doi:[10.1016/j.corsci.2010.08.021](https://doi.org/10.1016/j.corsci.2010.08.021)
- S. Ningshen, U. Kamachi Mudali, P. Mukherjee, A. Sarkar, P. Barat, N. Padhy, B. Raj, Influence of oxygen ion irradiation on the corrosion aspects of Ti-5 %Ta-2 %Nb alloy and oxide coated Titanium. *Corros. Sci.* **50**(8), 2124–2134 (2008). doi:[10.1016/j.corsci.2008.03.019](https://doi.org/10.1016/j.corsci.2008.03.019)
- P.M. Perillo, D.F. Rodríguez, The gas sensing properties at room temperature of TiO₂ nanotubes by anodization. *Sens. Actuators, B* **171–172**, 639–643 (2012). doi:[10.1016/j.snb.2012.05.047](https://doi.org/10.1016/j.snb.2012.05.047)
- S. Li, J. Qiu, M. Ling, F. Peng, B. Wood, S. Zhang, Photoelectrochemical characterization of hydrogenated TiO₂ nanotubes as photoanodes for sensing applications. *ACS Appl. Mater. Interfaces* **5**(21), 11129–11135 (2013). doi:[10.1021/am403325a](https://doi.org/10.1021/am403325a)
- V. Galstyan, E. Comini, G. Faglia, G. Sberveglieri, TiO₂ nanotubes: recent advances in synthesis and gas sensing properties. *Sensors* **13**(11), 14813–14838 (2013). doi:[10.3390/s131114813](https://doi.org/10.3390/s131114813)
- M.M. Byranvand, A.N. Kharat, M.H. Bazargan, Titania nanostructures for dye-sensitized solar cells. *Nano Micro Lett.* **4**(4), 253–266 (2012). doi:[10.1007/BF03353723](https://doi.org/10.1007/BF03353723)
- M. Boehme, W. Ensinger, Mixed phase anatase/rutile titanium dioxide nanotubes for enhanced photocatalytic degradation of methylene-blue. *Nano Micro Lett.* **3**(4), 236–241 (2011). doi:[10.1007/BF03353678](https://doi.org/10.1007/BF03353678)
- Y.B. Liu, H.B. Zhou, J.H. Li, H.C. Chen, D. Li, B.X. Zhou, W.M. Cai, Enhanced photoelectrochemical properties of Cu₂O-loaded short TiO₂ nanotube array electrode prepared by sonoelectrochemical deposition. *Nano Micro Lett.* **2**(4), 277–284 (2010). doi:[10.1007/BF03353855](https://doi.org/10.1007/BF03353855)
- L. Zheng, S. Han, H. Liu, P. Yu, X. Fang, Hierarchical MoS₂ nanosheet@TiO₂ nanotube array composites with enhanced photocatalytic and photocurrent performances. *Small* **12**(11), 1527–1536 (2016). doi:[10.1002/sml.201503441](https://doi.org/10.1002/sml.201503441)
- N. Gao, X. Fang, Synthesis and development of graphene-inorganic semiconductor nanocomposites. *Chem. Rev.* **115**(16), 8294–8343 (2015). doi:[10.1021/cr400607y](https://doi.org/10.1021/cr400607y)
- Y. Chen, J. Ni, H. Wu, R. Zhang, C. Zhao, W. Chen, F. Zhang, S. Zhang, X. Zhang, Study of cell behaviors on anodized TiO₂ nanotube arrays with coexisting multi-size diameters. *Nano Micro Lett.* **8**(1), 61–69 (2015). doi:[10.1007/s40820-015-0062-4](https://doi.org/10.1007/s40820-015-0062-4)
- Y. Lai, J. Huang, Z. Cui, M. Ge, K.Q. Zhang, Z. Chen, L. Chi, Recent advances in TiO₂-based nanostructured surfaces with controllable wettability and adhesion. *Small* **12**(16), 2203–2224 (2016). doi:[10.1002/sml.201501837](https://doi.org/10.1002/sml.201501837)
- Y. Tang, Y. Zhang, J. Deng, J. Wei, H. Le Tam, B.K. Chandran, Z. Dong, Z. Chen, X. Chen, Mechanical force-driven growth of elongated bending TiO₂-based nanotubular materials for ultrafast rechargeable lithium ion batteries. *Adv. Mater.* **26**(35), 6111–6118 (2014). doi:[10.1002/adma.201402000](https://doi.org/10.1002/adma.201402000)
- L. Qin, Q. Chen, R. Lan, R. Jiang, X. Quan, B. Xu, F. Zhang, Y. Jia, Effect of anodization parameters on morphology and photocatalysis properties of TiO₂ nanotube arrays. *J. Mater. Sci. Technol.* **31**(10), 1059–1064 (2015). doi:[10.1016/j.jmst.2015.07.012](https://doi.org/10.1016/j.jmst.2015.07.012)
- Y. Alivov, M. Pandikunta, S. Nikishin, Z.Y. Fan, The anodization voltage influence on the properties of TiO₂ nanotubes grown by electrochemical oxidation. *Nanotechnology* **20**(22), 225602–225608 (2009). doi:[10.1088/0957-4484/20/22/225602](https://doi.org/10.1088/0957-4484/20/22/225602)
- D. Regonini, F.J. Clemens, Anodized TiO₂ nanotubes: effect of anodizing time on film length, morphology and photoelectrochemical properties. *Mater. Lett.* **142**, 97–101 (2015). doi:[10.1016/j.matlet.2014.11.145](https://doi.org/10.1016/j.matlet.2014.11.145)
- S.P. Albu, P. Roy, S. Virtanen, P. Schmuki, Self-organized TiO₂ nanotube arrays: critical effects on morphology and growth. *Israel J. Chem.* **50**(4), 453–467 (2010). doi:[10.1002/ijch.201000059](https://doi.org/10.1002/ijch.201000059)
- R. Beranek, H. Hildebrand, P. Schmuki, Self-organized porous titanium oxide prepared in H₂SO₄/HF electrolytes. *Electrochem. Solid State Lett.* **6**(3), B12–B14 (2003). doi:[10.1149/1.1545192](https://doi.org/10.1149/1.1545192)
- H. Tsuchiya, J.M. Macak, A. Ghicov, L. Taveira, P. Schmuki, Self-organized porous TiO₂ and ZrO₂ produced by anodization. *Corros. Sci.* **47**(12), 3324–3335 (2005). doi:[10.1016/j.corsci.2005.015.04](https://doi.org/10.1016/j.corsci.2005.015.04)
- H. Tsuchiya, J.M. Macak, A. Ghicov, A.S. Räder, L. Taveira, P. Schmuki, Characterization of electronic properties of TiO₂ nanotube films. *Corros. Sci.* **49**(1), 203–210 (2007). doi:[10.1016/j.corsci.2006.05.009](https://doi.org/10.1016/j.corsci.2006.05.009)
- A. Hazra, K. Dutta, B. Bhowmik, P.P. Chattopadhyay, P. Bhattacharyya, Room temperature alcohol sensing by oxygen vacancy controlled TiO₂ nanotube array. *Appl. Phys. Lett.* **105**(8), 081604–081608 (2014). doi:[10.1063/1.4894008](https://doi.org/10.1063/1.4894008)
- A. Hazra, B. Bhowmik, K. Dutta, P.P. Chattopadhyay, P. Bhattacharyya, Stoichiometry, length, and wall thickness optimization of TiO₂ nanotube array for efficient alcohol sensing. *ACS Appl. Mater. Interfaces* **7**(18), 9336–9348 (2015). doi:[10.1021/acsami.5b01785](https://doi.org/10.1021/acsami.5b01785)
- P. Acevedo-Pe-a, L. Lartundo-Rojas, I. González, Effect of water and fluoride content on morphology and barrier layer properties of TiO₂ nanotubes grown in ethylene glycol-based electrolytes. *J. Solid State Electrochem.* **17**(11), 2939–2947 (2013). doi:[10.1007/s10008-013-2212-2](https://doi.org/10.1007/s10008-013-2212-2)
- F. Schmidt-Stein, S. Thiemann, S. Berger, R. Hahn, P. Schmuki, mechanical properties of anatase and semi-metallic TiO₂ nanotubes. *Acta Mater.* **58**(19), 6317–6323 (2010). doi:[10.1016/j.actamat.2010.07.053](https://doi.org/10.1016/j.actamat.2010.07.053)
- J. Moon, H.-P. Hedman, M. Kemell, A. Tuominen, R. Punkkinen, Hydrogen sensor of pd-decorated tubular TiO₂ layer prepared by anodization with patterned electrodes on SiO₂/Si substrate. *Sens. Actuators, B* **222**, 190–197 (2016). doi:[10.1016/j.snb.2015.08.054](https://doi.org/10.1016/j.snb.2015.08.054)
- D.H. Kim, Y.S. Shim, H.G. Moon, H.J. Chang, D. Su et al., Highly ordered TiO₂ nanotubes on patterned substrates: synthesis-in-place for ultrasensitive chemiresistors. *J. Phys. Chem. C* **117**(34), 17824–17831 (2013). doi:[10.1021/jp405150b](https://doi.org/10.1021/jp405150b)
- J. Moon, H.-P. Hedman, M. Kemell, A. Tuominen, E. Mäkilä, H. Kim, A. Tuominen, R. Punkkinen, A study of monitoring hydrogen using mesoporous TiO₂ synthesized by anodization. *Sens. Actuators, B* **189**, 246–250 (2013). doi:[10.1016/j.snb.2013.05.070](https://doi.org/10.1016/j.snb.2013.05.070)
- O.K. Varghese, M. Paulose, C.A. Grimes, Long vertically aligned titania nanotubes on transparent conducting oxide for highly efficient solar cells. *Nat. Nanotechnol.* **4**(9), 592–597 (2009). doi:[10.1038/nnano.2009.226](https://doi.org/10.1038/nnano.2009.226)
- S.L. Lim, Y. Liu, J. Li, E.T. Kang, C.K. Ong, Transparent titania nanotubes of micrometer length prepared by anodization of titanium thin film deposited on ITO. *Appl. Surf. Sci.* **257**(15), 6612–6617 (2011). doi:[10.1016/j.apsusc.2011.02.087](https://doi.org/10.1016/j.apsusc.2011.02.087)

31. H.A. Hamedani, S.W. Lee, A. Al-Sammarraie, Z.R. Hesabi, A. Bhatti, F.M. Alamgir, H. Garmestani, M.A. Khaleel, Synthesis and growth mechanism of thin-film TiO₂ nanotube arrays on focused-ion-beam micropatterned 3D isolated regions of titanium on silicon. *ACS Appl. Mater. Interfaces* **5**(18), 9026–9033 (2013). doi:[10.1021/am402203m](https://doi.org/10.1021/am402203m)
32. K.N. Chappanda, Y.R. Smith, M. Misra, S.K. Mohanty, Site-specific and patterned growth of TiO₂ nanotube arrays from e-beam evaporated thin titanium film on Si wafer. *Nanotechnology* **23**(38), 385601 (2012). doi:[10.1088/0957-4484/23/38/385601](https://doi.org/10.1088/0957-4484/23/38/385601)
33. K.N. Chappanda, Y.R. Smith, S.K. Mohanty, L.W. Rieth, P. Tathireddy, M. Misra, Growth and characterization of TiO₂ nanotubes from sputtered Ti film on Si substrate. *Nanoscale Res. Lett.* **7**, 388–395 (2012). doi:[10.1186/1556-276X-7-388](https://doi.org/10.1186/1556-276X-7-388)
34. S. Farsinezhad, A.N. Dalrymple, K. Shankar, Toward single-step anodic fabrication of monodisperse TiO₂ nanotube arrays on non-native substrates. *Phys. Status Solidi A* **211**(5), 1113–1121 (2014). doi:[10.1002/pssa.201330649](https://doi.org/10.1002/pssa.201330649)
35. S. Ono, M. Saito, H. Asoh, Self-ordering of anodic porous alumina induced by local current concentration: burning. *Electrochim. Solid State Lett.* **7**(7), B21–B24 (2004). doi:[10.1149/1.1738553](https://doi.org/10.1149/1.1738553)
36. Y. Li, M. Zheng, L. Ma, W. Shen, Fabrication of highly ordered nanoporous alumina films by stable high-field anodization. *Nanotechnology* **17**(20), 5101–5105 (2006). doi:[10.1088/0957-4484/17/20/010](https://doi.org/10.1088/0957-4484/17/20/010)
37. X. Yuan, M. Zheng, L. Ma, W. Shen, High-speed growth of TiO₂ nanotube arrays with gradient pore diameter and ultrathin tube wall under high-field anodization. *Nanotechnology* **21**(40), 405302–405311 (2010). doi:[10.1088/0957-4484/21/40/405302](https://doi.org/10.1088/0957-4484/21/40/405302)
38. S.P. Albu, A. Ghicov, S. Aldabergenova, P. Drechsel, D. LeClere, G.E. Thompson, J.M. Macak, P. Schmuki, Formation of double-walled TiO₂ nanotubes and robust anatase membranes. *Adv. Mater.* **20**(21), 4135–4139 (2008). doi:[10.1002/adma.200801189](https://doi.org/10.1002/adma.200801189)
39. A. Valota, D.J. LeClere, P. Skeldon, M. Curioni, T. Hashimoto, S. Berger, J. Kunze, P. Schmuki, G.E. Thompson, Influence of water content on nanotubular anodic titania formed in fluoride/glycerol electrolytes. *Electrochim. Acta* **54**(18), 4321–4327 (2009). doi:[10.1016/j.electacta.2009.02.098](https://doi.org/10.1016/j.electacta.2009.02.098)
40. D. Yu, X. Zhu, Z. Xu, X. Zhong, Q. Gui, Y. Song, S. Zhang, X. Chen, D. Li, Facile method to enhance the adhesion of TiO₂ nanotube arrays to Ti substrate. *ACS Appl. Mater. Interfaces* **6**(11), 8001–8005 (2014). doi:[10.1021/am5015716](https://doi.org/10.1021/am5015716)
41. R.P. Antony, T. Mathews, S. Dash, A.K. Tyagi, B. Raj, X-ray photoelectron spectroscopic studies of anodically synthesized self-aligned TiO₂ nanotube arrays and the effect of electrochemical parameters on tube morphology. *Mater. Chem. Phys.* **132**(2–3), 957–966 (2012). doi:[10.1016/j.matchemphys.2011.12.041](https://doi.org/10.1016/j.matchemphys.2011.12.041)
42. J. Wang, Z.Q. Lin, Anodic formation of ordered TiO₂ nanotube arrays: effects of electrolyte temperature and anodization potential. *J. Phys. Chem. C* **113**(10), 4026–4030 (2009). doi:[10.1021/jp811201x](https://doi.org/10.1021/jp811201x)
43. H. Yin, H. Liu, W.Z. Shen, The large diameter and fast growth of self-organized TiO₂ nanotube arrays achieved via electrochemical anodization. *Nanotechnology* **21**(3), 035601–035608 (2010). doi:[10.1088/0957-4484/21/3/035601](https://doi.org/10.1088/0957-4484/21/3/035601)
44. S.P. Albu, P. Schmuki, Influence of anodization parameters on the expansion factor of TiO₂ nanotubes. *Electrochim. Acta* **91**, 90–95 (2013). doi:[10.1016/j.electacta.2012.12.094](https://doi.org/10.1016/j.electacta.2012.12.094)
45. C.C. Chen, S.J. Hsieh, Evaluation of fluorine ion concentration in TiO₂ NT anodization process. *J. Electrochem. Soc.* **157**(6), K125–K130 (2010). doi:[10.1149/1.3374640](https://doi.org/10.1149/1.3374640)
46. R. Kojima, Y. Kimura, M. Bitoh, M. Abe, M. Niwano, Investigation of influence of electrolyte composition on formation of anodic titanium oxide nanotube films. *J. Electrochem. Soc.* **159**(11), D629–D636 (2012). doi:[10.1149/2.003211jes](https://doi.org/10.1149/2.003211jes)
47. Y. Sorachon, K. Woraphong, P. Nutdanai, Effect of anodization parameters on morphologies of TiO₂ nanotube arrays and their surface properties. *J. Chem. Chem. Eng.* **6**, 686–691 (2012)
48. K. Zhu, N.R. Neale, A. Miedaner, A.J. Frank, Enhanced charge-collection efficiencies and light scattering in dye-sensitized solar cells using oriented TiO₂ nanotubes arrays. *Nano Lett.* **7**(1), 69–74 (2007). doi:[10.1021/nl062000o](https://doi.org/10.1021/nl062000o)
49. J. Wang, Z. Lin, Freestanding TiO₂ nanotube arrays with ultra-high aspect ratio via electrochemical anodization. *Chem. Mater.* **20**(4), 1257–1261 (2008). doi:[10.1021/cm7028917](https://doi.org/10.1021/cm7028917)
50. V.V. Yakovlev, G. Scarel, C.R. Aita, S. Mochizuki, Short-range order in ultrathin film titanium dioxide studied by raman spectroscopy. *Appl. Phys. Lett.* **76**(9), 1107–1110 (2000). doi:[10.1063/1.125953](https://doi.org/10.1063/1.125953)
51. B.D. Fraters, E. Cavaliere, G. Mul, L. Gavioli, Synthesis of photocatalytic TiO₂ nano-coatings by supersonic cluster beam deposition. *J. Alloys. Compd.* **615**(1), S467–S471 (2014). doi:[10.1016/j.jallcom.2013.12.037](https://doi.org/10.1016/j.jallcom.2013.12.037)